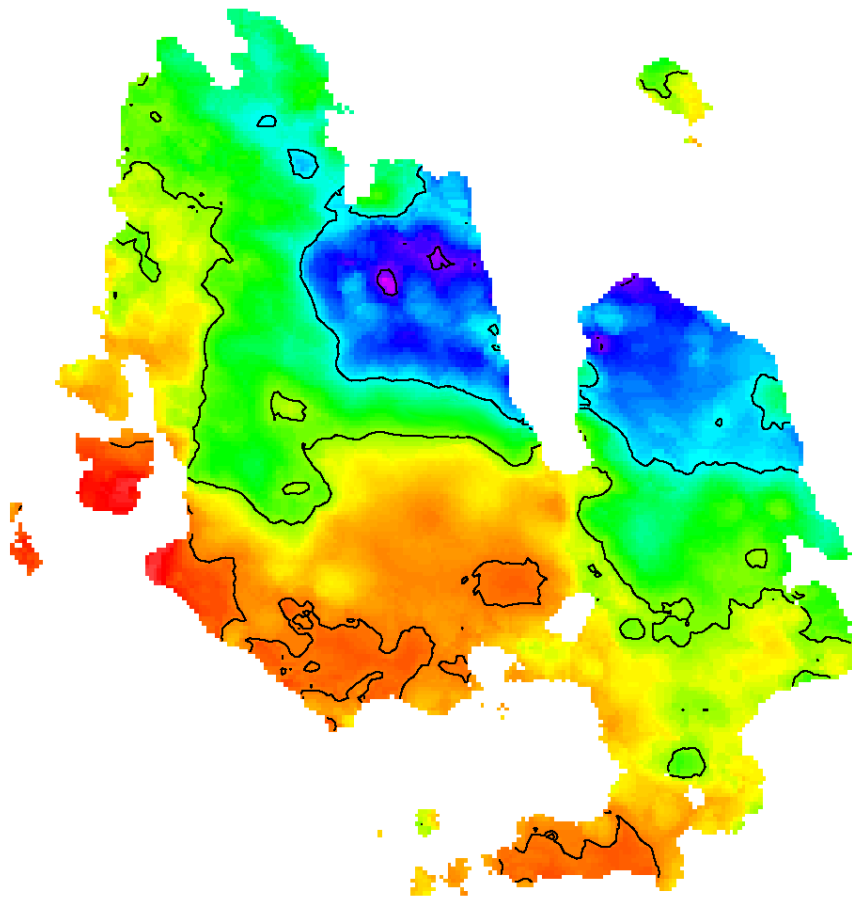


Staring into the eye of the Medusa

Lukas Lindroos, lindroos@student.chalmers.se

November 30, 2011

Supervisors:
Susanne Aalto
Sebastien Müller



Abstract

The Medusa is a nearby merger galaxy. The galaxy harbours an ongoing starburst with very efficient conversion of hydrogen to stars. This seems to happen despite the lack of high density gas. In this project I have studied the dynamics and structure of the molecular gas by looking at the rotational CO 2–1 line. I used data recorded with the SMA interferometer.

The data from SMA has allowed me to push the resolution to approximately $0''.4$ and generate the highest resolution molecular gas map of the Medusa yet. At this scale we have been able to observe giant molecular associations (GMAs). We find that the GMAs in general have larger velocity dispersion than what we would expect from their size. I will briefly discuss possible causes for this.

In the high resolution data we also find the Eye of the Medusa: a hole in the CO emission that is also associated with radio continuum emission and $H\alpha$. This seems to be the site of a dramatic star-forming event. The Eye of the Medusa is not located at the dynamical centre of the galaxy, but a few hundred parsecs out. Possibly where the inflowing gas meets the central rotation.

The new data has also allowed us a good look at the dynamics of the molecular gas. We found a quickly rotating central body with evidence of inflowing gas moving on non-circular orbits. We propose that what we see might be a molecular ring. This dynamical structure could be helping the starburst by rapidly feeding new gas into the centre.

Contents

1	Introduction	7
1.1	Star formation	7
1.2	The Medusa	8
1.3	Radio astronomy	8
1.4	Interferometry	10
1.5	Submillimeter array	10
2	Theory	13
2.1	Star formation tracers	13
2.2	Carbon monoxide as a tracer of molecular hydrogen	14
2.3	Mapping dynamics through redshift	15
2.4	Molecular associations	15
3	Method	17
3.1	Data reduction	17
3.1.1	The data	17
3.1.2	Calibration	18
3.1.3	Imaging and cleaning	18
3.2	Data analysis	19
3.3	Specifics	19
4	Results	21
4.1	Morphology	21
4.1.1	Morphology of isotopic variants	24
4.2	Kinematics	26
4.3	Molecular complexes	28
4.4	Center of the galaxy	31

Chapter 1

Introduction

“Twinkle twinkle little star. How I wonder what you are?”
Jane Taylor

As this old nursery rhyme witness the question what is up there has long intrigued thinkers. For a long time the stars seemed to be something that could impossibly be following the same laws of physics that we know here on earth.

However, the beginning of the 20th century saw huge leaps in understanding of the physical reality. Pioneers of physics and chemistry discovered the great energies inherent to the smallest particles. A source of energy capable of driving a star for billions of years was discovered here on earth. In a few decades it was more or less common knowledge that a star simply was a large collection of hydrogen fusing nuclei at the centre. This might seem to put an end to the wondering, but as always has been the case in science, with one question answered many more emerge.

The universe is a barren place, even near us inside the disc of the Milky Way, there are several light years of empty space around us. In this space there often a greater vacuum than can be obtained here at Earth. Can there really be enough stuff there to make a star?

A closer look reveals that the vast empty space is in fact swarming with molecules. Compared to Earth they may be very thinly spread, but on a galactic scale we still have a vast amount of gas. Understanding this dynamic becomes intimately connected with understanding star formation. And it is also here that many of the great questions of modern day astronomy lay.

1.1 Star formation

In our galaxy the Milky Way approximately one new star is formed each year (Robitaille & Whitney, 2010). This moderate rate of star formation is characteristic for galaxies similar to the milky way. Looking at other galaxies out there, using the tools we have to estimate star formation, not all galaxies behave this way.

Since galaxies vary in size we want to avoid simply looking at the star formation rate. If a more massive galaxy is forming more stars than a lighter one this is not very surprising. Therefor we often divide the star formation rate by

the mass of molecular gas in the galaxy. This gives us a new measure called the star formation efficiency.

Galaxies with very high star formation efficiency are called starburst galaxies. What is driving these galaxies to produce extra stars is today largely an open question. Many starburst galaxies are found at high redshift. Using Hubble's law that means large distances and light coming from an earlier time in the universe. These galaxies are interesting because they may be precursors to galaxies we see today. But they are often hard to study in detail. The large distance to these object means we can not get high resolution map of them. Also the radiation reaching Earth is faint.

For this reason we're trying to find more nearby galaxies that could be used as model galaxies for these more distant ones.

1.2 The Medusa

The Medusa (NGC4194) provides a good nearby example of a starburst galaxy. The amount of molecular hydrogen in the Medusa is in the same order of magnitude as the Milky Way (Dame, 1992; Aalto & Hüttemeister, 2000). Hancock et al. (2006) estimated the star formation rate in the Medusa to $\sim 46M_{\odot}/\text{yr}$ using $\text{H}\alpha$ lines. This is a dramatic difference from the earlier mentioned value of $1M_{\odot}$ per year for the milky way. It is located at approximately 39 Mpc away from us which in astronomical scales has to be considered close.

Simply looking at the optical image of the galaxy, see figure 1.1, indicates that something dramatic is going on. We can see the beginning of shell like structures to the south and tidal tail going out to the north. This seems to indicate that this is a collision between a smaller spiral galaxy and a larger elliptical one (Aalto & Hüttemeister, 2000).

Many galaxies seems to follow the Schmidt-Kennicutt law for star formation. This simplified mean that dense gas is more efficient at forming stars than less dense gas. According to the Schmidt-Kennicutt law we would expect a large amount of very dense gas. More dense gas means more chemistry and molecules like HCN should be easy to detect. However measurements done by Aalto & Hüttemeister (2000) did not detect any HCN and as such the Medusa appears to violate the Schmidt-Kennicutt law.

In this study I will try to use new data on molecular hydrogen (more specifically CO 2-1, a tracer for molecular hydrogen) to shed light on what is happening in the Medusa. More on that later, first a short introduction to radio astronomy.

1.3 Radio astronomy

When you look up at the sky night time you see a picture completely dominated by stars. Since we are more interested in the structures that forms new stars rather than the stars this is problematic. Fortunately starlight does not dominate on all wavelengths. The electromagnetic spectrum is large and all the way from gamma rays to radio we receive emission from space.

Moving into the radio regime of the EM spectrum we start finding molecular lines from the colder molecules in space. Typical example of such colder

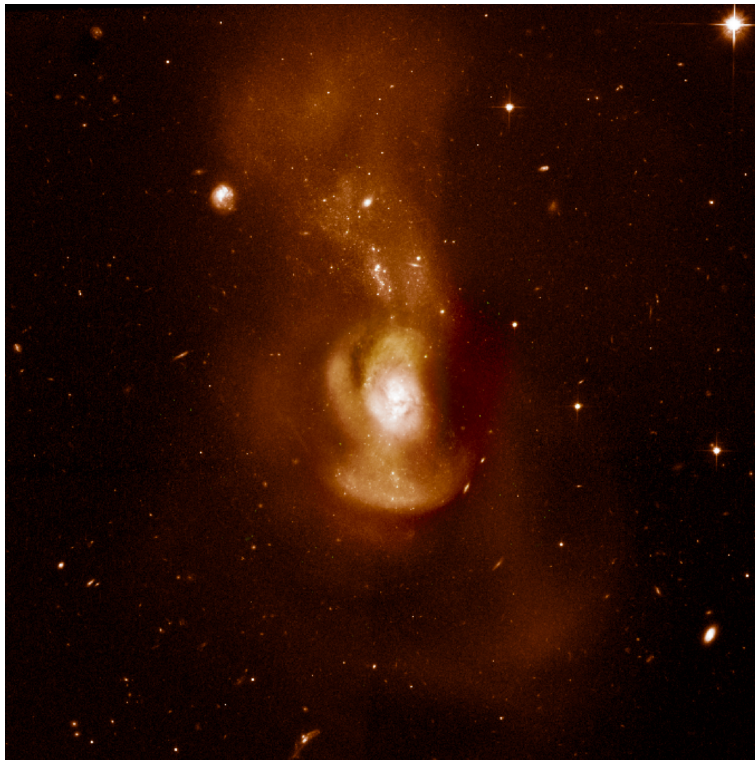


Figure 1.1: Image of the Medusa merger taken by HST.

molecules are found inside molecular clouds. Molecular clouds mainly consist of molecular hydrogen. The hydrogen molecules are not easy to detect as long as they are cold. However these regions give shelter and allow other molecules to form, some of these are much easier to detect.

These molecular clouds are exactly what we are interested in. They are the nurseries for new stars. The abundance of cold hydrogen form the environment where new stars can form.

One molecule of major importance is carbon monoxide. It is one of the easier molecules to form and has bright rotational lines to allow us to see it. Outside of molecular clouds it quickly gets broken apart by radiation. On the other hand if we have dense enough molecular hydrogen it will be protected and can gather in large amounts. Zooming in on these lines we will form a picture of the sky completely dominated by the molecular hydrogen regions rather than stars.

Moving into the radio regime of observational astronomy of course requires another kind of instrumentation. Traditional telescopes are replaced by antennas and receivers. This means both advantages and disadvantages.

One large advantage with radio astronomy worth mentioning is how simple it is to measure the frequency of a signal. Compared to optical astronomy extracting spectral information in radio is more or less automatic. This make molecular lines in radio perfect for studying dynamics of structures in space. We can use the spectral information to calculate the redshift (and thereby the

line of sight velocity) of all the emission we observe.

1.4 Interferometry

In modern submillimeter radio astronomy parabolic antennas are used to collect radiation. The size of these dishes will not only determine how much radiation they pick up but also their directionality. By increasing the size of the dish we will limit the angular area where it picks up radiation. This relation can be well approximated as

$$\delta = \frac{\lambda}{D} \quad (1.1)$$

where D is the diameter of the dish, λ is the wavelength observed, and δ is the resolution in radians. Dishes can vary in size from a few meters up a few hundred meters. Normally building dishes larger than 100 m isn't practical and most are smaller than that.

But a smaller dish of say 10 m is limited to an angular resolution of only 27 arc seconds at 230 GHz. For comparison this is approximately the size that Jupiter has when it is at its furthest point. With even the largest planets in our solar system appear as point sources it would be hard to achieve the goal of this research project.

However there is a way around this problem. By putting up several dishes and combining the data much better resolution can be achieved. The method used to combine the data is called interferometry, it relies on being able to both measure the phase and amplitude of the signal. This makes the radio regime ideal for interferometry.

The drawback here is that the total collection area is still rather small. As the dishes are spread more thinly the part of the sky that radiation is collected from will decrease. This means that the further apart the dishes are placed the lower the sensitivity.

1.5 Submillimeter array

In this study the primary source of data is the submillimeter array or SMA. The SMA is an array of antennas on top of the Mauna Kea. Mauna Kea is an over 4000 meter high volcano on Hawai. At this altitude there is much less water vapor in the atmosphere than at sea level. For submillimeter astronomy this is very important since water vapor absorbs radio waves, especially when you move towards submillimeter wavelengths.

In the SMA there are 8 antennas. As mention in section 1.4 there is a compromise to be done when placing these. Spreading them to thin will not give enough sensitivity but placing them to tight will lead to unsatisfactory resolution. Since some studies will have higher requirements on resolution and others on sensitivity it is possible to move the antennas. On the Mauna Kea there is a large number of pads for antennas. The antennas are then moved between different pads as different experiments require.

Generally the antennas are kept in one of four configurations: subcompact, compact, extended and very extended. With the subcompact having the best

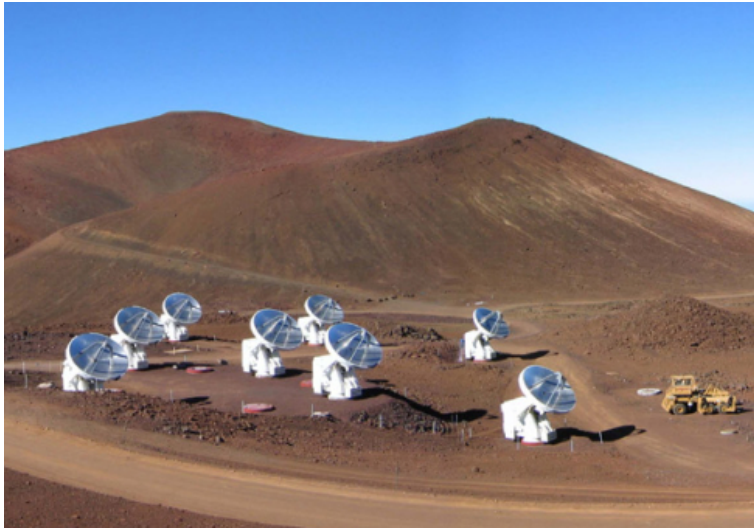


Figure 1.2: Image of the SMA on top of Mauna Kea

sensitivity and very extended the highest angular resolution. The longest baseline is approximately 70 meter for the compact configuration and roughly 500 meters for the very extended configuration.

The dishes in the SMA are relatively small at 6 meters. Since the angular resolution is determined by the array setup small dishes give the advantage with larger field of view. That is to say that the part of the sky that the array can map in one go increases.

Chapter 2

Theory

In this chapter I will try to go through some basic theory useful for understanding what I am going over in later chapters. But first I will go through some terminology.

Emission from the sky is generally measured as flux, this is the electromagnetic flux hitting Earth at a specific frequency. It is measured in Jansky where a Jansky is $10^{-26} \text{ W m}^{-2} \text{ Hz}^{-1}$. When flux maps are made we will be mapping the flux from a region of the sky called the beam. The beam can be thought of as the resolution element in radio astronomy, if we have a point source it will be smeared over this region. The pixels in a radio picture is often smaller than the beam so it is important to note that two adjacent pixels aren't independent.

The data from an array is usually processed to make the beam as close to a gaussian as possible. Unfortunately this is not always possible. A sidelobe is an additional image of a source that is off from the source position. The sidelobes will usually be much weaker than the main image but for a strong source the sidelobes can still become significant. This means that finding a weak source close to a stronger one is very difficult, there is a big risk that it simply gets obscured by sidelobes.

The flux measure is often converted to brightness temperature. This is the black body temperature needed to achieve this flux at a given frequency.

Another important concept is optical depth. Optical thickness is a measure of the transparency of a medium. If the medium is optically thin you will be able to see what is behind it, on the other hand it will be hard to actually see the object. As optical thickness then increases you will in the end only see the source and nothing of what is behind. If you increase the optical thickness further now the front of the source will obscure the back so you can not see it. This means that at this point the measured flux from a source will not increase if you increase the size or the density. Such a source we call optically thick.

2.1 Star formation tracers

When the stars are formed we can expect all sizes to be formed. The more massive of these stars will burn out much faster than smaller ones. This means a young population of stars will have more massive stars than an older population.

The most massive stars are called O-stars. At approximately ten times the

mass of our sun they will ionise a large region around them. This ionised gas will recombine and emit distinct radiation, primarily H α lines (Stahler & Palla, 2004). By looking at this radiation we can calculate the concentration of O-stars (Hancock et al., 2006). From this concentration we can then estimate the age of the stars and star formation rate.

Star formation is often found in regions with large amounts of dust. When the stars form they will heat this dust, the heating dust will emit radiation in the IR part of the spectrum. This means that we can use it to measure star formation (Condon, 1992). Especially the far (low frequency) infrared luminosity, L_{FIR} , is used.

2.2 Carbon monoxide as a tracer of molecular hydrogen

As mentioned before rotational transitions for CO is a convenient way to image molecular gas in space. CO is a linear molecule, that is one of the moments of inertia is negligible and the other two equal. This is true for all diatomic molecules since they are cylindrically symmetric.

This means that we can quickly determine the rotational energy levels as

$$E = \frac{h}{8\pi^2 c I_B} J(J+1) \quad (2.1)$$

where I_B is the moment of inertia. Quantum selection rules require that J only change by one in a transition. This means that a transition between J_1 and $J_2 = J_1 + 1$ will emit a photon with an energy of

$$\Delta E = \frac{h}{4\pi^2 c I_B} (J_1 + 1)$$

For CO this means we will have lines at 115.27 GHz, 230.54 GHz, etc. We call these lines by the syntax CO J_2 - J_1 , so the first is CO 1-0 and the second CO 2-1.

For the CO lines to be detected we need enough CO. As long as we have a relatively constant non-zero temperature the CO emissions will trace CO density more or less linearly. If the density get to high however the CO becomes optically thick. At this point we no longer see all the CO, and can only set a lower bound on the quantity of CO. CO 2-1 will be harder to excite than CO 1-0. This means we need higher temperature and density to see it than CO 1-0. This also mean that it will not as easily become optically thick.

As mentioned before the CO is amassed inside the protection of molecular clouds. Moving into the center of these clouds the CO lines will be optically thick. This unfortunately mean we can not estimate how much hydrogen is in the denser parts of the clouds using CO. However assuming that the clumps have a similar structure everywhere we can derive a global conversion factor. This will allow us a rough estimate of the total mass of molecular hydrogen in a galaxy. The exact conversion factor is a subject of much debate and varies with almost an order of magnitude between different publications. This mass estimate is still a useful tools to figure out approximately how much molecular gas we have.

2.3 Mapping dynamics through redshift

As mentioned earlier we can calculate the line of sight velocity from the red shift. In radio astronomy we define the line of sight velocity as

$$v_{\text{radio}} = c \frac{\nu_{\text{emit}} - \nu_{\text{obsv}}}{\nu_{\text{emit}}} \quad (2.2)$$

This formula is linear as you vary the line of sight velocity. The attentive reader will have noticed that this however differs from the more common formula used by optical astronomers:

$$v_{\text{opt}} = c \frac{\nu_{\text{obsv}} - \nu_{\text{emit}}}{\nu_{\text{obsv}}} \quad (2.3)$$

It is important to keep this difference in mind as you compare red shift measurements from radio and optical astronomy. But when looking at the relative velocities inside a galaxy the difference is not severe.

2.4 Molecular associations

The molecular clouds are structure with sizes around 50pc, with giant molecular clouds a bit larger (Goldsmith, 1987). Considering the angular resolution of SMA and distance to the Medusa it will be hard to probe these scales. However even at sizes around 100pc the molecular hydrogen can stay in gravitationally bound structure. At these scale they are called (giant) molecular associations.

As long as the structures are bound they will stabilize in virial equilibrium. That is the kinetic energy will be the same as the potential energy. We can use this to calculate the mass of the structure, if we only can measure the size and velocity dispersion. The mass found using this estimate is called virial mass.

Chapter 3

Method

This chapter will be dedicated to discussing the methods and algorithms needed to take data from antennas and extract physical information.

The first section is dedicated to discussing how the data from the antennas are processed into images. Then I will discuss how these images can be analysed to sort out the interesting information in a compact and useful form. In the last part of this chapter I will quickly go through the specifics for this project. Which calibrators were used and similar information.

3.1 Data reduction

In modern astronomy the concept of data reduction is important. That is taking the raw data and producing sky maps. With a interferometric array there are several important steps to this. I will discuss this from a perspective of SMA, but similar procedures would apply to other radio arrays.

The steps taken include three main steps.

1. Calibration
2. Imaging
3. Cleaning

I will discuss all these three steps but first a quick discussion of the data.

3.1.1 The data

A data point in interferometry is called a visibility. This is a measurement of how well in phase the signal coming to two different antennas is in phase at a specific frequency. Measuring this quantity is partly done because it is relatively easy to measure, but it also happens to correspond to a point in the fourier plane of the flux image.

For a visibility to make sense it has to be measured for a specific frequency. This means that we have to run the signal through a narrow bandpass. There is nothing preventing us from calculating the visibilities at several frequencies using several band passes. This means that a modern receiver will give us the visibilities for a number of frequencies (or channels).

3.1.2 Calibration

Even if the SMA is located at a high altitude the atmosphere is still not negligible. The uneven atmosphere will introduce an error in the relative phases as measured between the different antennas. This effect can be corrected for by using a calibrator. The antennas are aimed at a well known point source and the visibilities are measured. Since the source is a point source the visibility should only depend on the length of the baseline. Phase and amplitude errors of the different antennas can then be calculated. As the atmosphere changes over time we will have to redo this calibration at a regular interval while we are recording or data.

To do this it is however important to find a good calibrator source. If the source is too far away from the intended object of study it will not give a very good calibration. Another important aspect is the flux of the source, it has to be bright enough and have a stable flux. Quasars are generally considered good calibrators since they're very bright point sources and quite a few are known. They can however change their flux quite drastically. The changes over a measuring track should not be too significant, however from day to day it may change. To help this another source of well known flux can be used to first find the absolute flux level of the quasar. For this purpose the planets of our Solar System and their moons are often used. They are fewer than the quasars and less point like but the mechanism of their emission is well understood and work well for this purpose.

The noise is not necessarily the same for all frequencies. Using a bright quasar we can calibrate for this too. Knowing that the spectrum should be more or less flat for the quasar over the bandwidth of SMA we can tune the different channels to achieve this.

3.1.3 Imaging and cleaning

After calibration the visibilities still need to be turned into a real image of the source. As mentioned before it can be shown that each visibility measures a point in the Fourier transformation of the source. The point will be located at (u, v) in the Fourier plane (often called uv-plane in interferometry) where u and v are the separation of the antennas orthogonal to the source direction.

Unfortunately this way of sampling the Fourier plane doesn't give a perfect coverage. This can be modeled as having multiplied the data with a sampling function that is zero where there is no data and one where there is. When we try to take the inverse Fourier transform to get the real image we will get a convolution with the Fourier transform of the sampling function. This means it can sometimes be hard to sort out how the real source looks like. There are several methods to try to rectify this problem, most of them based on the algorithm proposed by Högbom (1974). These algorithms often all called CLEAN have shown themselves to be an effective way of converting the dirty image to a clean image.

Another complication is introduced by the fact that not all baselines are equivalent. The longer baselines are noisier but will be more important for small features. Since we're already removing the sampling function we might as well add a weight function to the data that we can remove in the CLEAN algorithm. Using this we can either maximize the resolution by weighting up

long baselines or get higher sensitivity by the inverse. There is two commonly used weighting modes used here.

Natural weighting is used to get maximal sensitivity in the map. The disadvantage with this weighting is that it will be decremental to the resolution since the longest baselines are all but ignored. If high resolution is more important uniform weighting can be used instead. Inversely we will now have trouble with the map getting noisy.

It is also possible to try to compromise by using a weighting mode called robust.

3.2 Data analysis

Once we have managed to reduce the data we will end up with one image per channel. At the large number of channels for SMA we end up with thousands of pictures of the sky at different frequency. To be able to make sense of this we have to reduce the amount of data.

We can start by picking out the part of the spectrum we are actually interested in. By summing up all the frequency bins corresponding to a line we get the zero moment map.

If we have a line emission we can also calculate higher order moment maps. The first moment is calculated as

$$M_1 = \frac{\int vI(x, y, v)dv}{M_0} \quad (3.1)$$

where M_1 is the first moment, M_0 is the zeroth moment and $I(x, y, v)$ is the emission for the position (x, y) and velocity v . This gives us a map of the average velocity of the gas.

The second moment is defined as

$$M_2 = \frac{\int v^2I(x, y, v)dv}{M_0} \quad (3.2)$$

and gives us the average velocity dispersion of the gas.

The moment maps give quick access to how some spectral properties change over the galaxy. When we have identified regions of interest we can extract exact spectra there.

3.3 Specifics

The CO 2-1 data in this report is based on two tracks recorded by the SMA. One track in very extended configuration taken on February 21 2010 and the other track in compact configuration 8 April 2010. The weather conditions were good for both tracks.

The compact track of 10 hours recorded system temperatures between 160K and 270K. The phase calibration was done using the quasar 1153+72, bandpass calibration on 3C454.3 and absolute flux calibration on Ganymede. The very extended track had system temperatures in the range 100K to 180K. The phase calibration was done using 1153+72, 0927+390 and 0721+713, bandpass calibration on 0854+201 and absolute flux calibration on Vesta.

All the calibrations were done using the `idl` software. The data was then reduced using `GILDAS` (<http://www.iram.fr/IRAMFR/GILDAS>). I also used `ROOT` (root.cern.ch) to work with the spectra and `octave` (octave.org) for some simpler plotting.

The very extended track and compact tracks were combined to make the ^{12}CO maps while isotopic variants were mapped using only the compact track. The continuum channel was subtracted in the `uv`-plane. To be able to make the higher resolution maps data was combined using a lower weight on the compact baselines. The data from SMA had a velocity resolution of roughly 1 km/s. This was smoothed to 16.9 km/s (adding 16 adjacent channels) before cleaning.

Chapter 4

Results

In this chapter I will start with discussing the morphology of the CO emission. I'll follow up with a discussion of the observed dynamics of the gas. Then I'll go back to look at the emission coming from smaller scale structures and try to identify molecular associations. Finally I will attempt to zoom in on the center of the galaxy.

4.1 Morphology

In figure 4.1 I present a moment zero map of the new data. The resolution in this map is comparable to that of the high resolution map of CO 1–0 presented by Aalto & Hüttemeister (2000) ($1''.7$ in Aalto & Hüttemeister (2000) compared to $1''.69 \times 1''.63$).

CO emission is spread over the central $15''$ of the Medusa. The brightest feature is about $1''$ south west of the 1.4GHz continuum peak as measured by Beswick et al. (2005). This feature stretches up towards the north east following the dust lanes going here.

To the right of these features we find another structure which appears to be separated from the center. It has a north south orientation with a size of approximately $10'' \times 3''$. Looking at a HST image of the galaxy there appears to be matching feature in the optical body of the galaxy.

The total flux of the CO 2–1 map is 339 Jy km/s. To avoid noise contributing significantly to this flux measure, signals weaker than 38 mJy ($= 5\sigma_{\text{noise}}$) were ignored in each velocity bin of 16.9 km/s. Of this 96% of the flux is concentrated to the central two features. In CO 1–0 Aalto & Hüttemeister (2000) found that 67% of the flux was in the center.

The non-central emission in the CO 1–0 was mostly spread in patches up to the north of the core. There is some CO 2–1 emission to the north as well. The morphology does not resemble that found in CO 1–0 and flux coming from the region is significantly lower. This would indicate that the gas in this region is colder and/or less dense in this region than the center. However it is also possible that we are losing some of the flux in the noise.

The total flux measured at 339 Jy km/s is very close to the value found by Casoli et al. (1992). They measured it to 66 K km/s in a beam of $13''$, 339 Jy km/s is 67 K km/s in the same beam.

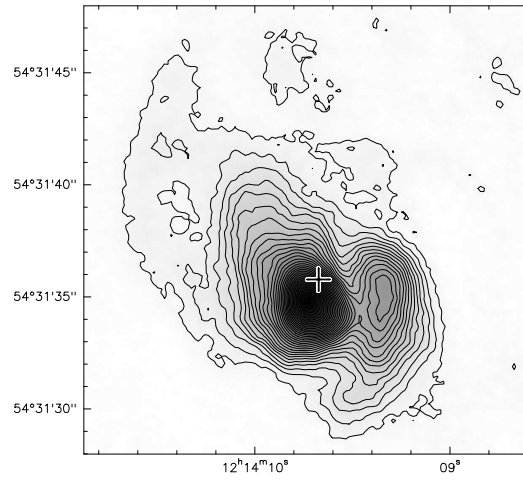


Figure 4.1: The zeroth moment map of CO 2-1 from Medusa in K km/s. Contours at three sigma of the noise in the map or 15 K km/s. The image is constructed by combining the compact and very extended track. This is then made into an image with a robust weighting of 9. The cross marks the location where emission peaks in radio continuum.

The peak flux is measured to 482 K km/s in our beam, this is more than 30 times the noise level in the map. This seems to indicate that we should be able to push the resolution further. Just changing the weighting scheme to uniform does not improve the resolution very much. To push it further I instead choose to increase the weight on the baselines from the very extended track. This allowed me to form the map seen in figure 4.2. The total flux in this map is still $\sim 340\text{Jy km/s}$ using a similar cut off at 5 sigma of the noise in each bin. In other words we are still recovering most of the flux albeit in a noisier map.

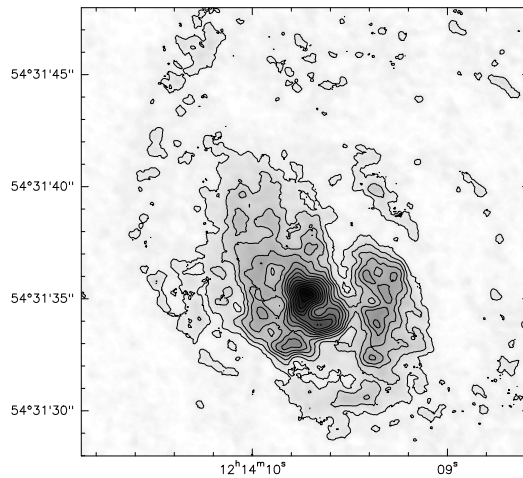


Figure 4.2: The zeroth moment map of CO 2-1 from Medusa (contours) in K km/s. Contours at three sigma of the noise in the map or 15 K km/s. Beam size of $0''.81 \times 0''.61$. The image is constructed by combining the compact and very extended track using a higher weight on baselines from the very extended track. This is then made into an image with a robust weighting of 5. The cross marks the location where emission peaks in radio continuum.

In this $0''.5$ map we get a much better idea of the actual structure of the CO. The tail going out to the north east is clearly structured in filaments.

There appears to be a depression in the center of the CO emission, a structure I will call the Eye of the Medusa. The Eye is not centered around the radio continuum peak making it unlikely that it is a dynamical structure. Rather it is probably the result of an event that has consumed, ionised or scattered that molecular gas.

The event that come to mind that would cause this is a starburst. Hancock et al. (2006) found a very high amount of $\text{H}\alpha$ emission from this region which would support this. We can also look for signs of this in radio continuum. The starburst would generate massive stars that would quickly go supernova. Supernovae remnants can be seen in radio continuum. Doing an overlay of the CO 2-1 on top of the 1.4 GHz continuum map done by Beswick et al. (2005) we find a striking resemblance, see figure 4.3: where the eye is located we have

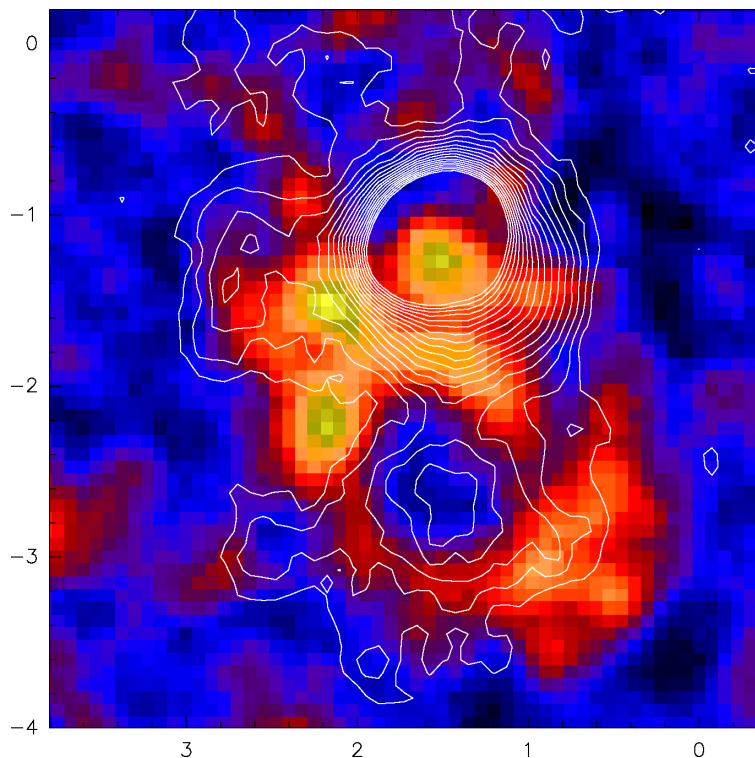


Figure 4.3: The zeroth order moment map of the CO 2-1 (colour) in a beam of $0''.37 \times 0''.43$ map overlaid on top of 1.4 GHz continuum (contours) measurement done by Beswick et al. Beswick et al. (2005). Beam size of continuum map is $0''.446 \times 0''.320$. The radio continuum peaks both at the supposed AGN and inside the ring found in ^{12}CO .

a clear peak in radio continuum.

From the map by Beswick et al. (2005) I determined that approximately 7% of the 1.4GHz continuum flux was coming from this region. This gives a star formation rate of approximately $0.4 M_{\odot}$ per year using the formula of Condon (1992). Hancock et al. (2006) have also measured the star formation in this region. Using $\text{H}\alpha$ they have determined a star formation rate to $16 M_{\odot}$ per year, 40 times more than the value we found. This very large difference seems to indicate that $\text{H}\alpha$ measure is overestimating the SFR.

4.1.1 Morphology of isotopic variants

The wide bandwidth of SMA allows us to search for isotopic variants of CO. Using only the compact data we have been able to detect both ^{13}CO 2-1 and C^{18}O 2-1. See figure 4.4 for a map of ^{13}CO 2-1 flux. If we calculate a total flux from this map we get $\sim 10 \text{ Jy km/s}$ using the same algorithm as with ^{12}CO fluxes. Unfortunately this measure is strongly dependent on the noise of the map, reducing the cut off flux in the bins to $3\sigma_{\text{noise}}$ the measured total flux increases to 20 Jy km/s .

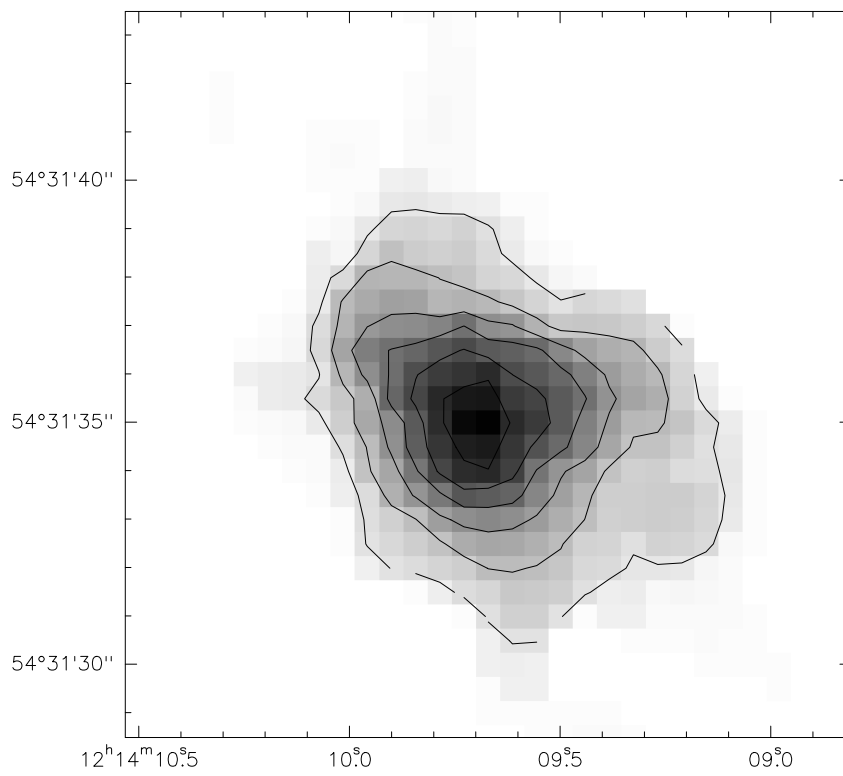


Figure 4.4: Map of ^{13}CO 2-1 flux from the Medusa. Fluxes from 0 to 26 K km/s. Contours at $3\sigma_{\text{noise}}$ where $\sigma_{\text{noise}} \approx 1.3\text{K km/s}$. Beam is $3''.33 \times 3''.25$.

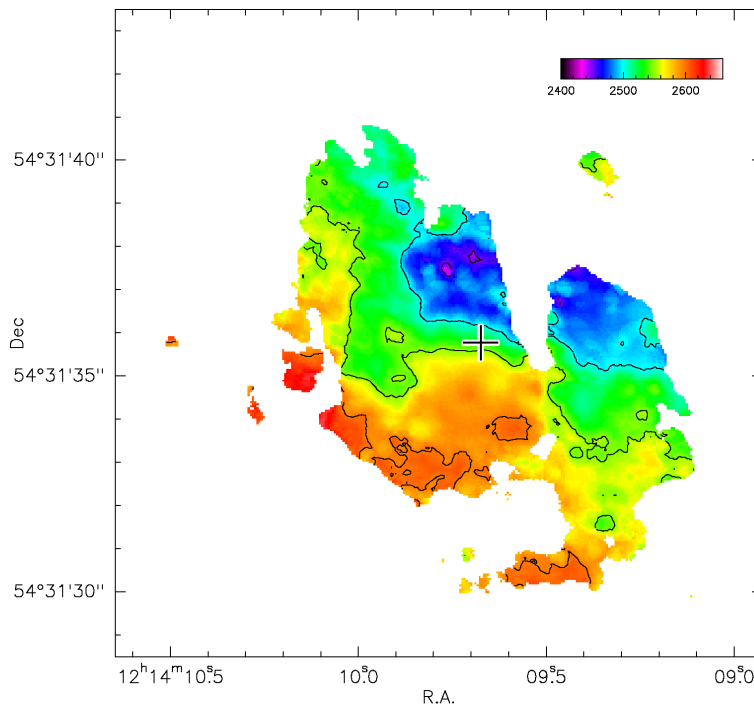


Figure 4.5: The first moment map of the Medusa. Calculated from CO 2–1 map with velocity resolution of 16 km/s, noise level of 6.45 mJy/beam. Beam size of $0''.81 \times 0''.61$. Radio continuum peak marked in the middle.

Clearly we are losing flux in the edges of the distribution, but that does not mean that the center of the distribution is not correctly measured. Here the flux is stronger and the noise contribution should be less. The peak flux is 26 K km/s which is over $20\sigma_{\text{noise}}$. Using the compact data we can determine the peak position and flux in ^{12}CO as well. The position is off with $0''.7$, not significant considering the beam size of roughly $3''$. The flux ratio of the peak fluxes is approximately 12.

Now switching over to C^{18}O we get a four sigma detection of this. The peak flux is measure to 7.6 K km/s in a beam of $3''.37 \times 3''.21$ giving a ^{12}CO 2–1 over C^{18}O 2–1 flux ratio of 40.

4.2 Kinematics

Looking at the first moment map, figure 4.5, we see a general north-south rotation. The upper side rotating towards us and the lower side away from us.

We expect the dynamical center of the galaxy to be close to where radio continuum emission peaks. Zooming in around here we see a structure with a very regular rotation. This structure appears to have a major axis with a position angle of approximately 20° (angle from y-axis in mathematically positive direction). Guided by this I have taken a pv-cut along this axis cutting through the radio continuum peak flux, see figure 4.6.

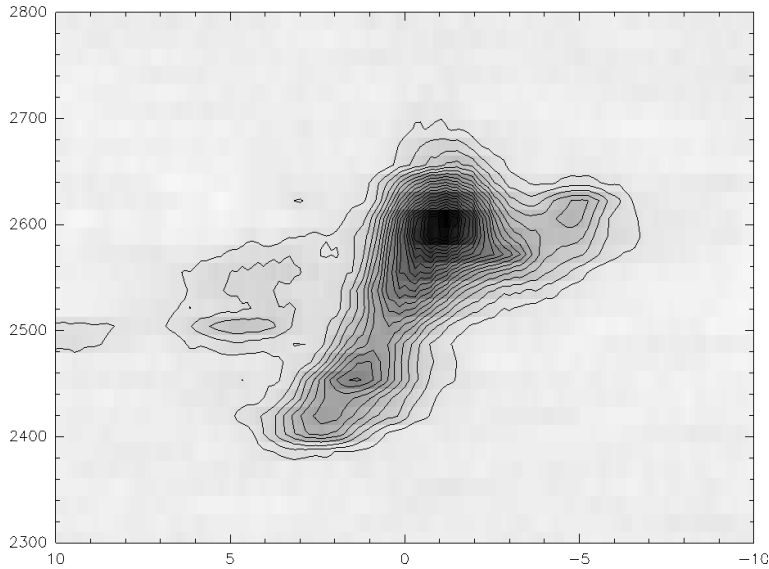


Figure 4.6: Position-velocity cut along a PA of 20° . The origin is located at radio continuum peak, slit width of $1.6''$ and beam size of $1.69'' \times 1.63''$. Positive direction is north.

The x-like shape in the pv-cut is similar to what you would find if there was a bar present (Garcia-Burillo & Guelin, 1995). However looking at the HST images we see no indication of a bar-like structure. A possible explanation for this is that we have a molecular ring rather than a bar.

Either way, most of the gas is caught in this structure, rotating as a solid body. Seen as the straight line in the pv-diagram. The gas in this structure appears to be present until a radius of approximately $3''$. A straight line drawn along the ridge gives a velocity gradient of ~ 60 km/s per arc second or ~ 300 km/s/kpc. Guessing at an inclination of this structure of approximately 45° this would mean a total rotation speed of 252 km/s at the edge or a rotation time of 14 million years.

To the north and south of the core we have lagging behind main structure at lower velocity. This will allow this gas to move in towards the center of the galaxy. When this falls in towards the center it will be accelerated in the gravity potential of the galaxy. For some gas to actually stick in the center it will need to be slowed down. This could be achieved when the gas collides with the ring(/bar/central structure).

The Eye of the Medusa is located where the inflowing gas would be merging with the central rotation. If the gas falling into the galaxy get stuck here it would help explain why such a large fraction gas is gathered here. This could possible help explaining some of the $H\alpha$ flux coming from here. If the gas is colliding that would result in shock, and shocks would ionise gas.

4.3 Molecular complexes

By using uniform weighting I was able to push the resolution to $0''.43 \times 0''.37$, see figure 4.7. This allows us to probe structures down to a size of approximately $0''.4 \cdot 39\text{Mpc} = 75.6\text{pc}$. At this scale the CO emission should be clumpy and we will be able to resolve giant molecular associations.

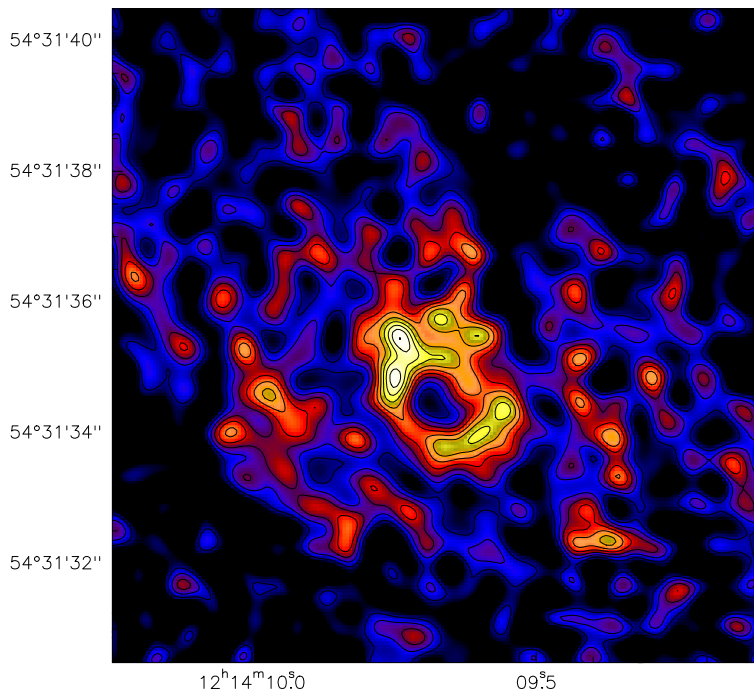


Figure 4.7: The zeroth moment map of CO 2-1 from Medusa in K km/s. Contours at one sigma of the noise in the map or 75 K km/s. Beam size of $0''.43 \times 0''.37$. The image is constructed by combining the compact and very extended track using a higher weight on baselines from the very extended track. This is then made into an image with a robust weighting of 1.

We do indeed see a clumpy structure, with most of the emission gathered around the Eye. The moment zero map show that there are several structures at over $3\sigma_{\text{noise}}$. We want to determine which of these are actual molecular complexes. There are several methods for identifying structure in a map such as this. A common way to do it is trying to fit gaussians close to peaks in the map. If a structure can be fitted with a three dimensional gaussian (two spatial and velocity) it probably is a coherent collection of gas.

I tried to use GAUSCLUMP algorithm in GILDAS MAPPING to do this. Combining this with the bad signal to noise in the high resolution map fitting gaussians was not possible.

Instead I resorted to identifying clouds by eye in the moment zero map. All larger structures with a peak flux over $3\sigma_{\text{noise}}$ in the center was assigned an approximate shape. I then removed all pixels that had less than half the peak intensity. I obtained a spectra by averaging the spectra in a 5×5 pixel area

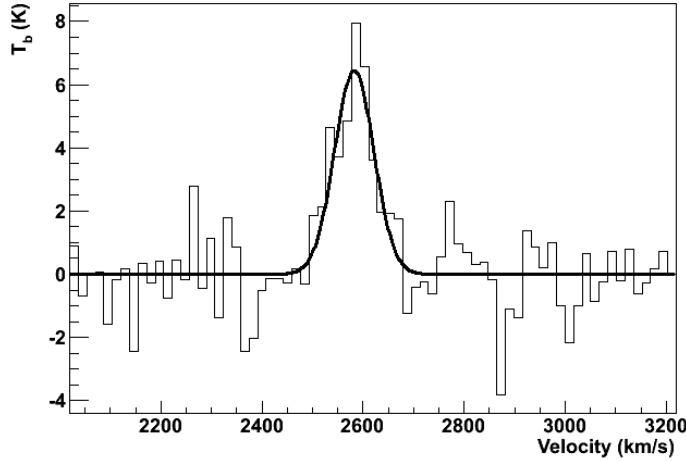


Figure 4.8: Spectra of a giant molecular association in the Medusa.

around the peak. For some typical spectra see figure 4.8 and 4.9.

All clouds that had no clear detection in the spectrum were removed at this point. To be able to estimate the virial mass of associations all clouds with double peaked spectrum were removed also. This left me with eight GMA.

Using the spectra that I obtained I fitted gaussians and determined line width of these GMA. Total brightness was estimated by summing in the moment zero map. Finally the size was determine by measuring the longest and shortest distance through center of the cloud, from edge to edge. The size used was then taken to be the average of these.

Looking at the clouds one thing come to mind. The associations have very large velocity dispersions comparing to what we would find in the Milky Way. Scoville & Sanders (1987) looked at structures inside the Milky Way and even for the largest structures the velocity dispersion did not come near what is in this data. Partly this may be facilitated by the rapid rotation of the center. If we assume the gas is rotating with the central structure we will get a velocity broadening of $0.4 \cdot 0.189 \cdot 300 \approx 22.7 \text{ km/s}$ I removed this amount from the velocity dispersion of the molecular associations located inside the center.

In figure 4.10 the result is visible. It appears that the velocity dispersion is still approximately twice as large as you would expect. The one association that seems to be on more Milky Way like velocity dispersion is a bit suspicious. I have subtracted 22.7 km/s from its velocity dispersion due to its location. But the measured average velocity of this clump of 2574 km/s does not put it in the right place in the pv-diagram to be following the central rotation. It is possible that this association is flowing inwards and this would mean that the true velocity dispersion is actually larger than 5.6 km/s.

Using this data I calculated mass for these associations using virial theorem and using CO brightness. I used a conversion factor $X = N(\text{H}_2)/I(\text{CO}) = 2.3 \cdot 10^{20} \text{ cm}^{-2} (\text{K km/s})^{-1}$ and a $M_{\text{vir}} = 660 D \sigma^2$. The association that stuck out in the size-line width sticks out here as well, having a much lower virial mass

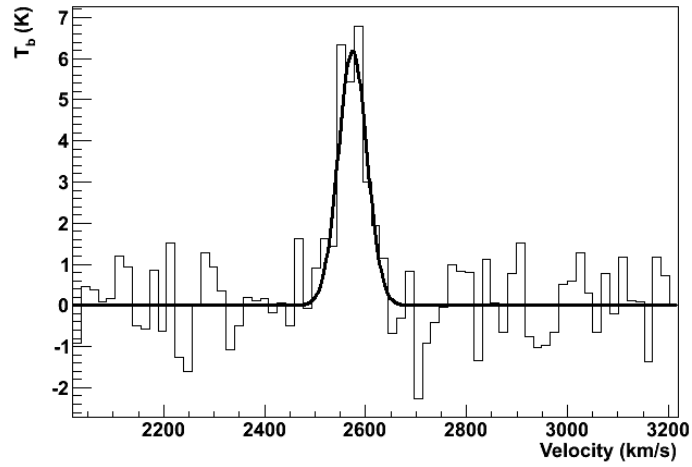


Figure 4.9: Spectra of a giant molecular association in the Medusa.

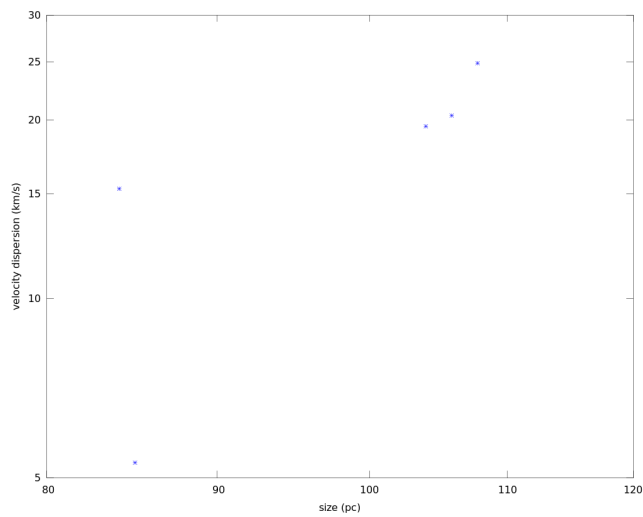


Figure 4.10: Size of clouds plotted versus the one dimensional velocity dispersion. The central rotation has been removed from the velocity dispersion of the central associations.

than CO mass. This again support that we are underestimating the velocity dispersion of this structure.

Up in the left side of the plot we have an association that has about three times higher CO mass than virial mass. This structure is located on the north side of the Eye of the Medusa in a region with alot of CO emission. It seems likely that either emission from other nearby structures is attributed to it or my estimate of size was far to strict.

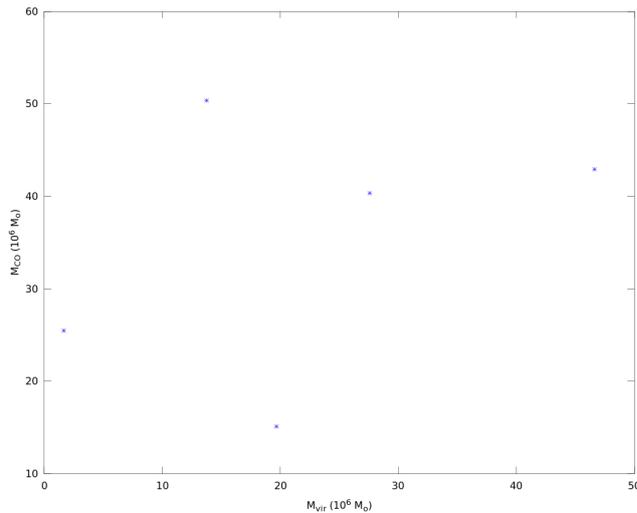


Figure 4.11: Virial mass compared to mass calculated from CO brightness.

The other three associations have very close values in both mass estimates. These estimate both indicate that they are very massive compared to similar sized structures in the Milky Way. Deciding to trust the virial mass leads to average densities of 618 cm^{-3} , 636 cm^{-3} and 964 cm^{-3} . however since we are looking at CO 2-1 it is possible that we underestimate the size of the structures. CO 2-1 will require higher density and temperature to get excited meaning that it will pushed towards the center of the associations.

4.4 Center of the galaxy

Looking at the high resolution map we find a feature just south of the radio continuum peak. This feature gives strongest signal at 12h14m9.68s $54^{\circ}31'35''54$. Looking at the spectrum here, see figure 4.12, we find two distinct velocity components.

Fitting gaussian function to these velocity components we determine the velocity of these features to 2420 km/s and 2594 km/s. This appears to represent gas rotating quickly around the central black hole. We are able to use standard Keplerian laws and assuming an inclination of 45° we are able to calculate the mass of the black hole.

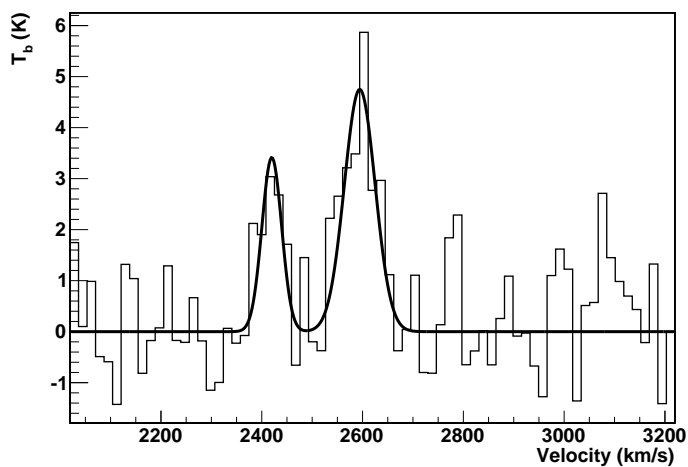


Figure 4.12: CO 2–1 spectrum close to the radio continuum emission peak. Produced from map with $0''.37 \times 0''.43$ resolution.

$$M = \frac{4\pi^2 r^3}{GT^2} = \frac{v^2 r}{G \cos^2 \alpha} = 268 \cdot 10^6 M_\odot$$

This feature appears inside the beam, meaning we are not resolving it. From this we can conclude that we are probably overestimating the radius. As such this is also too large value of the total mass of the black hole, but it is an upper bound.

It is also interesting to compare this spectrum to that found in HI absorption by Beswick et al. (2005). The smaller peak matches well with the HI spectrum, however the larger feature is completely missing. This seems to indicate that this gas is located behind the radio continuum source.

Bibliography

- Aalto, S., & Hüttemeister, S. 2000, *A&AS*, 362, 42
- Beswick, R. J., Aalto, S., Pedlar, A., & Hüttemeister, S. 2005, *ApJS*, 444, 791
- Casoli, F., Dupraz, C., & Combes, F. 1992, *A&A*, 264, 55
- Condon, J. J. 1992, *ARA&A*, 30, 575
- Dame, T. M. 1992, *AIP Conference Proceedings*, 278, 267
- Garcia-Burillo, S., & Guelin, M. 1995, *A&A*, 299, 657
- Goldsmith, P. F. 1987, in *Astrophysics and Space Science Library*, Vol. 134, *Interstellar Processes*, ed. D. J. Hollenbach & H. A. Thronson Jr., 51–70
- Hancock, M., Weistrop, D., Nelson, C. H., & Kaiser, M. E. 2006, *AJ*, 131, 282
- Högbom, J. A. 1974, *A&AS*, 15, 417
- Robitaille, T. P., & Whitney, B. A. 2010, *ApJ*, 710, L11
- Scoville, N. Z., & Sanders, D. B. 1987, in *Astrophysics and Space Science Library*, Vol. 134, *Interstellar Processes*, ed. D. J. Hollenbach & H. A. Thronson Jr., 21–50
- Stahler, S. W., & Palla, F. 2004, *The formation of stars*, 1st edn. (Weinheim: Wiley-VCH)